JCTC Journal of Chemical Theory and Computation

Origins of Resistance Conferred by the R292K Neuraminidase Mutation via Molecular Dynamics and Free Energy Calculations

Ricky Chachra[†,§] and Robert C. Rizzo*[,†,‡]

Department of Applied Mathematics and Statistics, and the Institute for Chemical Biology and Drug Discovery, Stony Brook University, Stony Brook, New York 11794

Received February 28, 2008

Abstract: Point mutations in the influenza virus enzyme neuraminidase (NA) have been reported that lead to dramatic loss of activity for known NA inhibitors including the FDA approved sialic acid mimics zanamivir and oseltamivir. A more complete understanding of the molecular basis for such resistance is a critical component toward development of improved next-generation drugs. In this study, we have used explicit solvent all-atom molecular dynamics simulations, free energy calculations (MM-GBSA), and residue-based decomposition to model binding of four ligands with NA from influenza virus subtype N9. The goal is to elucidate which structural and energetic properties change as a result of a mutation at position R292K. Computed binding free energies show strong correlation with experiment ($r^2 = 0.76$), and an examination of individual energy components reveal that changes in intermolecular Coulombic terms (ΔE_{coul}) best describe the variation in affinity with structure ($r^2 = 0.93$). H-bond populations also parallel the experimental ordering ($r = -0.96$, $r^2 = 0.86$) reinforcing the view that electrostatics modulate binding in this system. Notably, in every case, the simulation results correctly predict that loss of binding occurs as a result of the R292K mutation. Per-residue binding footprints reveal that changes in $\Delta\Delta E_{coul}$ for R292K-wildtype at position 292 parallel the change in experimental fold resistance energies ($\Delta\Delta G_{R292K\text{-}WT}$) with S03 < S00 < S02 < S01. The footprints also reveal that the most potent ligands have (1) less reliance on R292 for intrinsic affinity, (2) enhanced binding via residues E119, E227, and E277, and (3) flatter ΔE_{coul} and ΔH-bond profiles. Improved resistance for S03 appears to be a function of the ligand's larger guanidinium group which leads to an increased affinity for wildtype NA while at the same time a reduction in favorable interactions localized to R292. Overall, the computational results significantly enhance experimental observations through quantification of specific interactions which govern molecular recognition along the N9-ligand binding interface.

Introduction

Hemagglutinin (HA) and neuraminidase (NA) are glycoproteins on the surface of the influenza virus and, as integral to the life cycle of the virus, are attractive targets for drug design.[1] The World Health Organization (WHO) classifies the HAs into sixteen subtypes (H1−H16) and the NAs into nine subtypes (N1−N9) based on antigenic and genetic analysis.[1−3] Current flu vaccines are based on common circulating influenza A virus subtypes H1N1 and H3N2 and influenza B virus.[4] Overall, seasonal influenza causes an estimated 250,000−500,000 deaths worldwide and about 30,000−50,000 deaths in the United States each year.[4] Historically, prior pandemics include the 1918 Spanish flu (H1N1) with an estimated 50−100 million deaths,[5] the 1957

* Corresponding author e-mail: rizzorc@gmail.com.
† Department of Applied Mathematics and Statistics.
‡ Institute for Chemical Biology and Drug Discovery.
§ Current address: Weill Cornell Graduate School of Medical Sciences, Cornell University, New York, NY 10021.

10.1021/ct800068v CCC: $40.75
Published on Web 08/12/2008

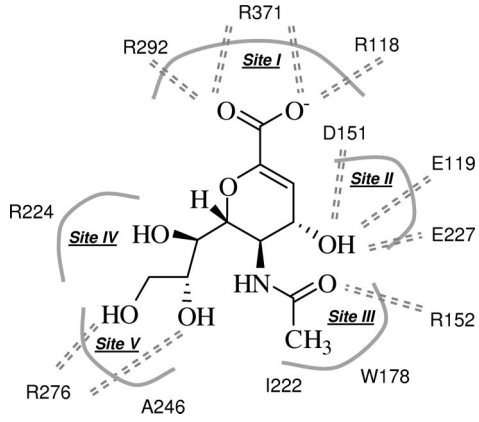

Figure 1. Key interactions in the neuraminidase active sites for inhibitor Neu5Ac2en (Table 1, S01). Figure adapted from ref 25 which divides the site into five regions (Site I−V). Specific hydrogen bonds and salt-bridge interactions are shown as dashed lines.

Asian flu (H2N2) with >1 million deaths, and the 1968 Hong Kong flu (H3N2) with ca. 700,000 deaths.[6] The more recent but highly pathogenic avian influenza A subtype H5N1, first isolated in 1998,[7] has an astounding mortality rate with 383 human cases and 241 deaths reported to WHO for the period 2003−June 1, 2008.[3] While HA is involved in binding of the virion to the host cell, NA cleaves terminal sialic acid groups from host cell-surface glycoproteins and glycolipids resulting in release of viral progeny and further spread of infection. A significant focus of drug design against influenza has involved development of derivatives of sialic acid designed to inhibit the release of viral progeny by binding to NA. Notably, numerous computational studies have aided these efforts,[8–20] and development of "flu" inhibitors is often cited as a seminal example of structure-based drug design.[21] To date, two NA inhibitors have been approved by the FDA,[22] oseltamivir and zanamivir, and a third compound, peramivir, is in phase 2 of clinical trials.[23]

In its biologically functional form, NA is a tetramer made of four identical subunits each of which contains a super-barrel structure primarily made of beta-sheets.[24] Each monomer contains an active site which Stoll et al.[25] have divided into five regions (Sites I−V) as shown in Figure 1. Overall the binding site is structurally well-conserved across subtypes and strains and is highly charged; nine of the twelve binding pocket residues in Figure 1 are charged. Of particular importance is the trio of Arg residues in Site I at positions 118, 292, and 371 which form strong hydrogen bonds with the carboxylate off of position C2 on the central ring of ligand substrates (see Table 1 for numbering).[8] It is important to note that this carboxylate group has been a key feature of all reported inhibitors of neuraminidase. The acetamido group (position C5) which interacts with Site III residues is also largely conserved in most inhibitors.

Although the active site of NA is largely conserved across all subtypes (N1−N9) and strains,[8] evolving point mutations in NA pose a major challenge for development of antivirals as several mutations are known to cause a serious loss of sensitivity to reported chemotherapeutics.[26–32] For instance, different strains with N1 subtypes bearing H274Y and N294S

Table 1. Chemical Structures and Inhibition Constants for Sialic Acid Analogs[a] with Wildtype (WT) and Mutant (R292K) Neuraminidase

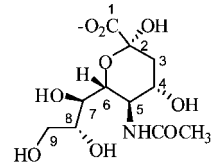

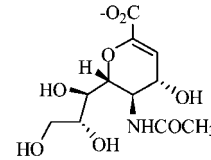

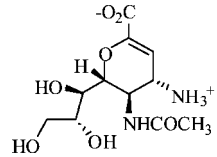

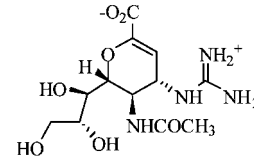

code	K_i-WT (μM)[b]	ca. ΔG_{WT} (kcal/mol)[c]	K_i-R292K (μM)[b]	ca. ΔG_{R292K} (kcal/mol)[c]	$\Delta\Delta G_{R292K\text{-}WT}$ (kcal/mol)
S00	55	−5.81	1820	−3.74	2.07
S01	2.64	−7.61	280	−4.85	2.76
S02	0.148	−9.32	14	−6.62	2.70
S03	0.002	−11.87	0.033	−10.21	1.66

[a] S00, *N*-acetylneuraminic acid (Neu5Ac, sialic acid); S01, 2-deoxy-2,3-dehydro-*N*-acetylneuraminic acid (Neu5Ac2en, DANA); S02, 4-amino Neu5Ac2en; S03, 4-guanidino Neu5Ac2en (zanamivir). [b] Experimental values from ref 26 for A/NWS/Tern/Australia/G70C (subtype N9). [c] Experimental free energies of binding (ΔG_{WT}, ΔG_{R292K}) estimated as ΔG_{bind} exptl $\approx$ RT ln (K_i in molar) at 25 °C.

mutations have been shown to confer up to 1800- and 200-fold resistance respectively to oseltamivir.[28,29] Point mutations known to adversely affect binding and activity for inhibitors with subtype N9 include R292K (Site I)[26] and E119G (Site II)[27] and to a lesser extent R152K (Site III).[30] Understanding the molecular basis for resistance caused by such deleterious mutations is critical for the development of more effective anti-influenza virus compounds.

McKimm-Breschkin et al.[26] have reported activities for a series of sialic acid mimics which inhibit NA from subtype N9 from influenza strain A/NWS/Tern/Australia/G70C for both the wildtype and R292K mutant. Table 1 shows structures, activities, free energies of binding (ΔG_{WT}, ΔG_{R292K}), fold resistance energies ($\Delta\Delta G_{R292K\text{-}WT}$), and code numbers for S00, *N*-acetylneuraminic acid (Neu5Ac, sialic acid); S01, 2-deoxy-2,3-dehydro-*N*-acetylneuraminic acid (Neu5Ac2en, DANA); S02, 4-amino-Neu5Ac2en; and S03, 4-guanidino-Neu5Ac2en (zanamivir, RELENZA[22]). S00 and the other three ligands differ at position C2 where S00 has a hydroxyl group which results in a nonplanar six-membered ring compared with the other compounds which contain double bonded character at position C2═C3 resulting in a more planar scaffold. Otherwise, the ligands differ only in functionality at position C4. S02 and S03 bear positively charged amino and guanidino functionality, respectively, while S00 and S01 contain a neutral OH group. The presence of a charged group at C4 has a significant effect on interaction of those ligands with residues in the binding site. The ligands in Table 1 are arranged in order of increasing

activity. All ligands show a substantial reduction in experimental activities due to the R292K mutation.[26] Although S03 (zanamivir) is the most potent, and the most resilient to R292K, the experimental fold resistance ($\Delta\Delta G_{R292K\text{-}WT}$) energies reveal that the weakest binder S00 is actually the second-most robust to the point mutation (Table 1, S03 > S00 > S02 > S01).

Characterizing binding for ligands with wildtype and mutant forms of NA will ultimately enable the design of improved inhibitors. Prior NA computational studies include rational design[8] using Goodford's GRID program,[33] energy minimization and molecular dynamics (MD),[9,11] Poisson-Boltzmann (PB) calculations,[10] linear interaction energy (LIE) calculations,[12] PMF-scoring using DOCK,[13] comparative binding energy analysis,[14] molecular orbital calculations,[15] MM-PBSA simulations,[16–18] QSAR analysis,[19] charge optimization,[34] and MD simulations aimed at characterizing loop flexibility[20] from recently crystallized[35] N1 subtypes. The present study is focused on characterization of the R292K variant. All-atom explicit solvent MD simulations, free energy calculations, and residue-based decomposition were used to model ligands in complex with NA subtype N9 with the following goals: (1) develop a robust computational model for prediction of binding affinities in agreement with experiment, (2) determine which factors contribute most to the observed binding affinities, and (3) delineate which specific structural and energetic factors contribute to the R292K resistance profiles. Well-tested computational models of inhibitors with N9, and clinically relevant mutants, will enable isolation of the energetic and structural determinates which confer improved binding resilience of S03 and a greater understanding of what drives molecular recognition with NA in general. Development of improved inhibitors across all NA subtypes, including the recently discovered highly pathogenic avian strain,[7] is paramount given the likelihood of future influenza pandemics.[6,36,37]

Theoretical Methods

In this study, free energies of binding were estimated for four ligands with wildtype neuraminidase and an R292K mutant using the single trajectory Molecular Mechanics Generalized Born Surface Area (MM-GBSA) method.[38,39] This approach was recently used to successfully investigate binding for a series of large viral entry peptide inhibitors of HIVgp41[40] and to determine the origins of selectivity for small inhibitors of matrix metalloproteases.[41] Although considered an approximate free energy calculation technique, the benefits include relative ease of setup and use, the ability to study large structural changes, and the ability to compare binding energies between ligands with diverse topologies. Tradeoffs include an incomplete accounting of all solute entropic effects and the fact that an implicit solvent model is used for the free energy calculations. However, changes in solute configurational entropies can be reasonably assumed to remain constant when ligands have similar binding poses and these changes are often ignored. Further, recent advances[42,43] and robust evaluation[44] of GBSA continuum methods for estimation of desolvation effects have revealed that implicit solvent models can indeed be very accurate provided that correct charge models and radii are employed in the calculations. Finally, the single trajectory method used here obviates the need for alchemical transformations to obtain free energies given that only a single simulation of each protein−ligand complex is required.[38,39] Thus, results can be obtained considerably faster than what are historically regarded as gold-standard free energy calculation methods which rely on perturbation techniques such as thermodynamic integration (TI) and free energy perturbation (FEP).[45,46] Despite the approximation made in MM-GBSA, the method has been used with good overall success to study a wide variety of problems.[18,40,41,47–50] The present study serves as an additional test of the utility of the method for estimation of the effects of point mutations on protein−ligand binding.

The calculations make use of explicit solvent MD simulations to generate ensembles of low energy structures which are postprocessed to compute the binding energy components. Implicit solvent is used only for estimation of the desolvation terms. After the simulations, explicit solvent is stripped off, and the coordinates for each species are separated to yield the complex, unbound receptor, and unbound ligand. Average energies (and associated uncertainties) are computed from many single point calculations using the ensemble of structures saved periodically during the MD simulations with each species total free energy estimated using eq 1. The total binding free energy is computed using eq 2.

$$G = \Delta G_{hyd} + E_{MM} - TS \quad (1)$$

$$\Delta G_{bind} = G_{complex} - (G_{receptor} + G_{ligand}) \quad (2)$$

Free energy of hydration ($\Delta G_{hyd} = G_{polar} + G_{nonpolar}$) terms which account for the desolvation penalties which occur upon binding are estimated from Generalized Born (GB) and Solvent Accessible Surface Area (SASA) calculations which yield G_{polar} and $G_{nonpolar}$, respectively. As validation, Rizzo et al.[44] have recently shown good agreement between experiment and theory from calculations of more than 500 organic molecules using continuum GBSA methods to estimate ΔG_{hyd}. The E_{MM} term represents the sum of electrostatic (Coulombic), van der Waals (Lennard-Jones), and internal energies (bonds, angles, and dihedrals) which are computed using the same molecular mechanics force field used during the original MD simulations. Using the single trajectory approximation, coordinates of separated ligand and receptor are identical to those in the complex, thus any changes in bond, angle, and dihedral (ΔE_{bond}, ΔE_{angle}, and $\Delta E_{dihedral}$) energies inherent in eqs 1 and 2 will cancel and ΔE_{coul} and ΔE_{vdw} reflect only the nonbonded intermolecular energies. The final TS terms, representing temperature (T) and solute entropy (S), were omitted given the consistent binding pose and size for the four NA ligands being studied. Neglecting $T\Delta S$ and internal strain energy is considered to be a reasonable approximation when ligands are of similar size and structure and only relative binding affinities are of interest. However, it should be emphasized that changes in

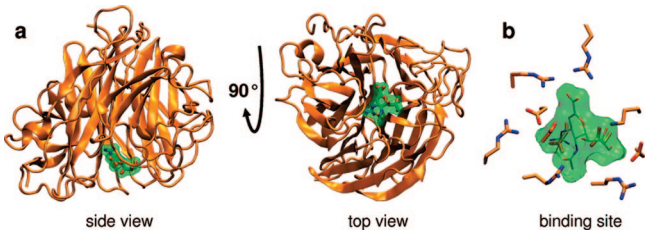

Figure 2. **(a)** Two views of neuraminidase (orange) complexed with ligand S03 (green). Protein coordinates from PDB entry 1F8B. **(b)** Close up view of the highly flexible and charged binding site.

system entropy due to the hydrophobic effect are in fact included as they are inherently contained in the ΔG_{hyd} terms.

Computational Details

System Setup. The biological form of NA is a tetramer; however, each monomer contains a functionally complete binding site,[1] thus only a single monomer was used for the simulations (Figure 2). The binding site is lined with highly charged and flexible Arg, Lys, Asp, and Glu residues. Receptor and ligand preparation was done using the Molecular Operating Environment (MOE) program.[51] The coordinates of neuraminidase subtype N9 complexed with ligand S01 were taken from the 1.80 Å crystallographic structure reported by Smith et al.[52] (pdb entry 1F8B) shown in Figure 2. The N9 receptor structure is from strain A/NWS/Tern/Australia/G70C which is the same strain employed in the experimental activity measurements reported by McKimm-Breschkin et al.[26] (see Table 1) and for the ligands being studied here. Crystallographic water molecules were deleted from 1F8B; however, a single calcium ion near the active site was retained.

Examination of available crystal structures for the 4 ligands complexed with wildtype NA and R292K shows the same well-defined binding pose, and protein side chain conformations in the NA binding site are relatively consistent across the series with the only primary difference being the rotameric state of Lys for the mutation. Therefore, a single set of receptor coordinates (in this case 1F8B with ligand S01) was used as the basis for construction of all simulations. This was primarily motivated by the fact that this would potentially eliminate noise in the simulations caused by multiple different starting conditions (i.e., multiple crystal structures). The R292K mutant was made by manually mutating Arg to Lys at residue 292 in 1F8B and orienting Lys to mimic the rotamer found in structures of R292K and avoid any steric clashes. Initial geometries for analogs S00, S02, and S03 were obtained from crystallographic complexes 2QWB, 2QWD, and 2QWE and oriented into the 1F8B reference frame (which contained S01) through alignment of C-alpha backbone atoms common to all NA structures. This procedure results in eight receptor−ligand complexes constructed from a single set of N9 coordinates.

The wildtype and R292K receptors were saved as PDB files without hydrogen atoms, and the ligands were saved as MOL2 files which included hydrogen atoms. Simulation ready parameter files were constructed for each system using the AMBER8 suite of programs.[53] The *antechamber* and *tleap* modules were used to assign the GAFF[54] force field parameters to the ligands and FF99SB[55] parameters and hydrogen atoms to the receptors. Protein side chains were assigned default AMBER protonation states (Asp/Glu minus, Arg/Lys ±) which, in the current study, yielded good results. A previous study by Masukawa et al.[16] similarly used default protonation states for NA, with a related AMBER force field, also with good success. The current work does not study changes in protonation; however, Smith et al.[52] and Fornabaio et al.[56] have reported computational results for NA under varying states. For the ligands, GAFF parameters were augmented with ChelpG[57] partial atomic charges computed at the HF/6-31G*//HF/6-31G* level of theory using the program Gaussian98.[58] Inspection of energy minimized ligands using the force field in the unbound state revealed a nonplanar guanidino group for S03 which was remedied through manual addition of GAFF improper dihedral angle parameters which forced the group to be planar. Each system was then subjected to a short energy minimization which yielded relatively small changes in geometry (bound and unbound) and no discernible steric clashes which indicated that the starting coordinates and force field parameters were reasonable.

MD Simulations and Postprocessing. Each solvated protein−ligand system contained 390 residues (including one calcium ion and the ligand) and 11,949 TIP3P[59] waters in a rectangular periodic box of 68 × 77 × 77 Å^3. All energy minimizations and MD employed the *sander* module from AMBER8. A nine step equilibration protocol was used prior to production MD in the following order. First, energy minimization for 1000 cycles followed by 50 ps of MD at 298.15 K was performed on each complex using a restraint weight of 5.0 kcal/mol Å^2 on all heavy atoms (steps 1 and 2). This was followed by three rounds of energy minimization for 1000 cycles each in which the restraint weight on heavy atoms was reduced from 2.0, to 0.1, to 0.05 kcal/mol Å^2 (steps 3−5). An additional three rounds of MD (50 ps each at 298.15 K) were performed with decreasing restraint weights reduced from 1.0, to 0.5, to 0.1 kcal/mol Å^2 (steps 6−8). A final equilibration of 50 ps of MD at 298.15 K using restraints only on protein backbone atoms (C-alpha, C, N, O) was then performed using a weight of 0.1 kcal/mol Å^2 (step 9). The production run employed the same weak backbone restraints as the last equilibration step for a total of 2000 ps of MD. A 1 fs time step was used for the equilibration stages (steps 1−9), and a 2 fs was used for the final production runs.

Weak backbone restraints were employed in the final production runs based on preliminary results from unrestrained MD simulations of NA monomers using only implicit solvent which showed larger than expected movement especially for protein termini regions. Larger motion would be expected due to a lack of friction in implicit solvent dynamics but is probably also a consequence of the fact that an NA monomer was simulated instead of a tetramer of NA subunits which would have otherwise held the protein termini restrained. In order to avoid similar artifacts in the explicit solvent TIP3P-MD, a weak restraint was employed to keep

the backbone fold intact. Weak restraints have previously been used with good results for simulations of inhibitors with MMPs[41] and HIVgp41.[40] Temperature and pressure of the simulations was regulated using the Berendsen[60] schemes using the heat bath coupling and pressure relaxation time constants of 1.0 ps each. The SHAKE[61] algorithm was applied to constrain bonds involving hydrogen atoms, and the particle mesh Ewald (PME)[62] method was used with 8.0 Å direct-space nonbonded cutoff.

Coordinates (snapshots) of each complex were saved every picosecond (2000 snapshots total) during the MD production trajectory. Each trajectory was then split into separate species representing the complex, the unbound receptor, and the unbound ligand, and the *sander* module was used to perform single point postprocessing calculations to compute the energy components (ΔE_{vdw}, ΔE_{coul}, $\Delta\Delta G_{polar}$, $\Delta\Delta G_{nonpolar}$) needed for estimation of the total binding free energy (ΔG_{bind} calcd). The polar energy terms G_{polar} were obtained via the AMBER implementation[63,64] of the Hawkins, Cramer, and Truhlar[65,66] pairwise Generalized Born[67] model as modified by Onufriev et al.[68] (model type igb=5). GB calculations employed dielectric constants of 1 and 78.5 and AMBER mbondi2 radii. Nonpolar terms were estimated as $G_{nonpolar} = \gamma SASA + \beta$ with SASA in Å^2 using standard values of $\gamma = 0.00542$ kcal/mol Å^2 and $\beta = 0.92$ kcal/mol.[69] Binding site footprints were obtained from pairwise decomposition of the per-residue interaction energies between the ligands and each NA residue and averaging over the total trajectory. Intermolecular hydrogen bonds were also computed and were defined as a structural interaction between a donor (H_D) and acceptor (X_A) with a distance of 2.5 Å or less and an angle between X_D-H_D---X_A of between 120 and 180°.

Results and Discussion

Simulation Stability. The stability of each simulation was monitored through examination of structural and energetic properties which occurred during the course of the 2 ns production trajectories. Figure 3, which is representative, shows results for ligand S01 complexed with wildtype neuraminidase. Here, plots of root-mean-square-deviation from the original starting coordinates (rmsd, Figure 3a), instantaneous changes in desolvation ($\Delta\Delta G_{hyd}$, Figure 3b), electrostatic (ΔE_{coul}, Figure 3c), and van der Waals (ΔE_{vdw}, Figure 3d) nonbonded interaction energies are well-behaved which indicate the simulations are reasonably converged. In particular, ΔE_{vdw} interactions remain almost constant across the trajectory, and rmsd values (Figure 3a) show only minor variation. Interestingly, a relatively small shift in ligand positional rmsd (Figure 3a, blue line) at around 300 ps results in a rather large increase in favorable ΔE_{coul} with a concurrent increase in unfavorable $\Delta\Delta G_{hyd}$. Such a large change in energy, from a relatively small change in geometry, is expected to be a consequence of the fact the NA binding site is so highly charged. After this change, the ligand rmsd remains constant, but the opposing desolvation and electrostatic terms then slowly come back to their respective equilibrium positions observed before the change. Another shift in group correlated energies for ΔE_{coul} with $\Delta\Delta G_{hyd}$ appears starting at around 1700 ps (Figure 3b vs Figure 3c).

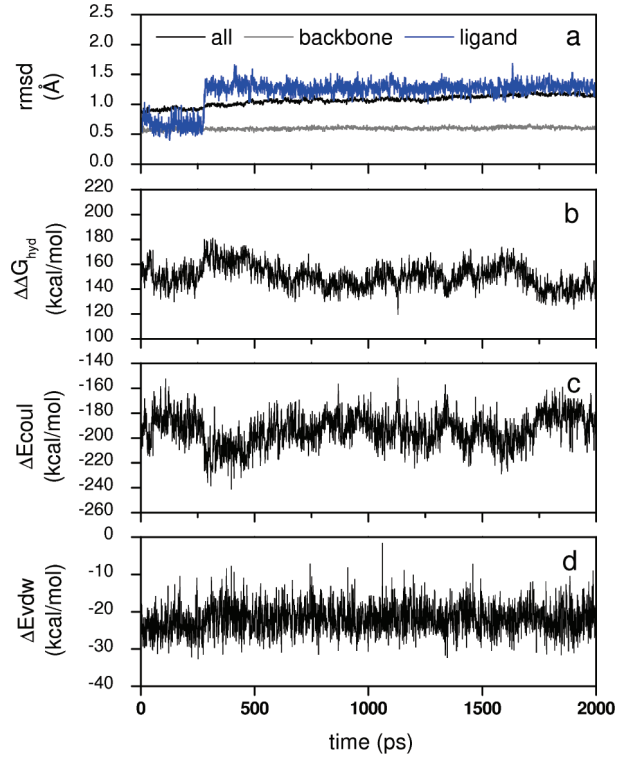

Figure 3. Instantaneous results from MD simulations of ligand S01 with wildtype neuraminidase subtype N9 plotted vs time. **(a)** shows root-mean-square deviation (rmsd) in angstroms (Å) between snapshots from the MD simulations and the initial starting coordinates for all protein heavy atoms (black line), protein backbone main chain atoms C-alpha, C, N, O (gray line), and ligand heavy atoms (blue line). **(b)** shows the change in free energy of hydration ($\Delta\Delta G_{hyd} = \Delta\Delta G_{polar} + \Delta\Delta G_{nonpolar}$), while panels **(c)** and **(d)** show the nonbonded intermolecular electrostatic (ΔE_{coul}) and van der Waals (ΔE_{vdw}) interaction energies, respectively.

For this second period, normal protein side-chain sampling is expected to be the primary factor given the relatively flat ligand rmsd shown in Figure 3a (blue line). In terms of magnitude, the nature of the highly charged NA binding site results in significantly more favorable ΔE_{coul} interaction energies than ΔE_{vdw} (Figure 3c vs Figure 3d). As discussed below, variation in computed electrostatic properties appear to play the dominant role in describing variation in the experimentally observed activities.

Our group and others have previously noted that favorable intermolecular electrostatic energies are anticorrelated to the opposing desolvation penalties.[11,40,41,70–73] Here, the correlation coefficient is computed to be $r = -0.86$ between $\Delta\Delta G_{hyd}$ and ΔE_{coul} for the 2000 instantaneous energies shown in Figure 3 for S01 with wildtype N9. The subtle interplay of structure with the various energy terms is a hallmark of the intimate relationship between opposing interactions (i.e., desolvation with electrostatics) which ultimately contribute to the overall free energy of binding. Notably, the present simulations and protocols appear to capture such subtleties well. The dramatic effects of desolvation are even more pronounced when considering all four ligands (S00−S03) with both receptors (wildtype and R292K). Here, an $r^2 =$

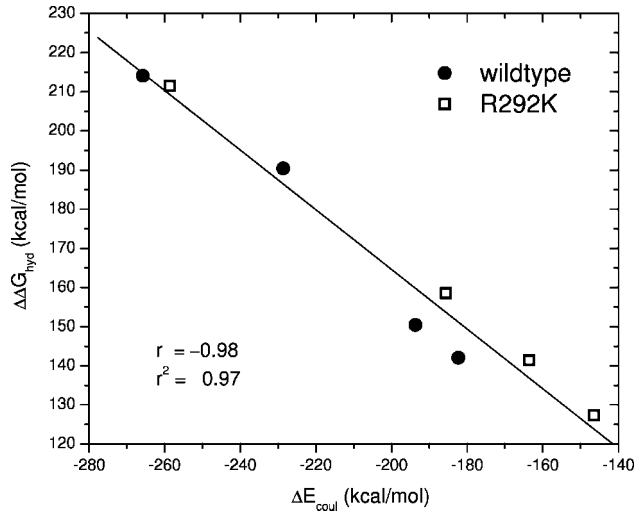

Figure 4. Intermolecular protein−ligand Coulombic energies (ΔE_{coul}) versus opposing desolvation penalties ($\Delta\Delta G_{hyd}$). Each symbol represents the average energy computed from 2000 MD snapshots saved during simulations of S00−S03 with wildtype (●) and R292K mutant (□) neuraminidase subtype N9.

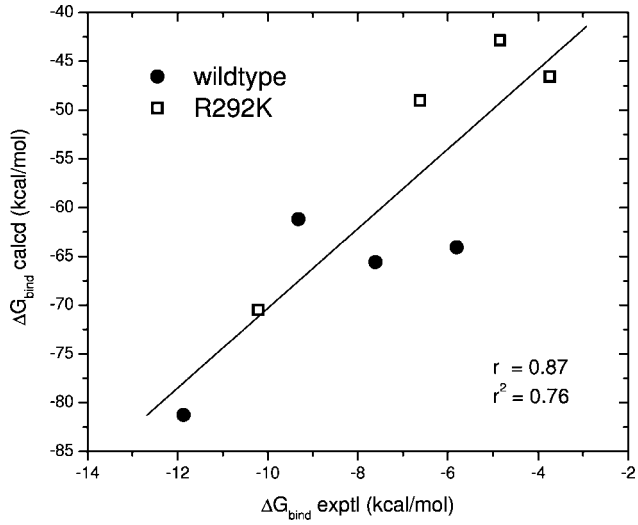

Figure 5. Average computed free energies of binding (ΔG_{bind} calcd) versus experimental activities (ΔG_{bind} exptl) for sialic acid inhibitors with wildtype (●) and R292K mutant (□) neuraminidase subtype N9.

0.97 is obtained using averaged values ($N = 2000$) for ΔE_{coul} and $\Delta\Delta G_{hyd}$ as shown in Figure 4.

Correlation with Experimental Activities. Figure 5 shows the correlation between the experimental (ΔG_{bind} exptl) and theoretical (ΔG_{bind} calcd) free energies of binding computed using the MM-GBSA method. Here, each data point represents the average values of ΔG_{bind} calcd obtained from 2000 MD snapshots of the four ligands with either wildtype (filled circles) or the R292K mutant (open squares), and the correlation coefficients of $r = 0.87$ and $r^2 = 0.76$ indicate overall good agreement with the experimental binding free energies. Notably, the calculations correctly predict that the R292K mutations reduced binding with each ligand in every case as highlighted in Figure 6 which shows instantaneous computed ΔG_{bind} values for wildtype (solid

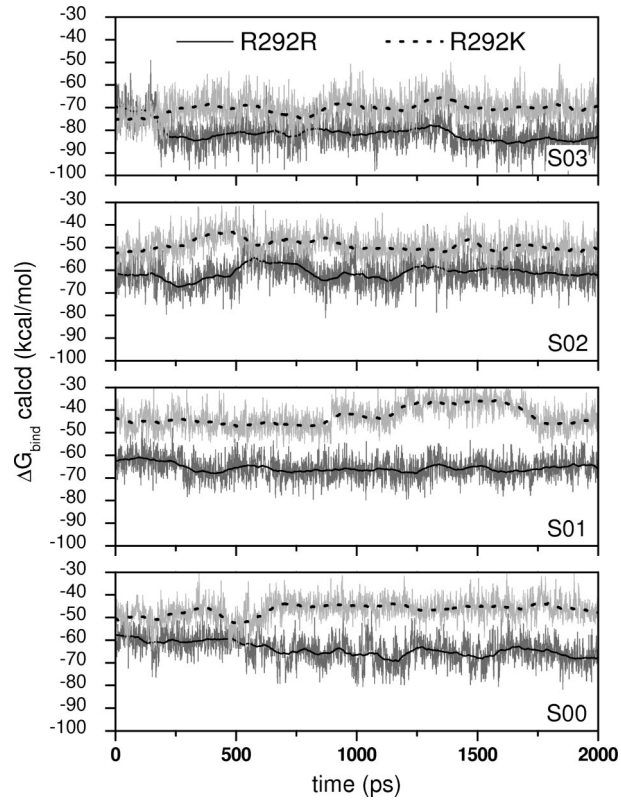

Figure 6. Instantaneous (jagged lines) and 100-block averaged (smoothed lines) free energies of binding (ΔG_{bind} calcd) vs time for ligands with wildtype (black, solid lines) and R292K (gray, dashed lines) neuraminidase subtype N9.

lines) and R292K (dashed lines) trajectories. As was observed in plots of individual energetic components (Figure 3), the total free energies (ΔG_{bind} calcd $= \Delta E_{vdw} + \Delta E_{coul} + \Delta\Delta G_{hyd}$) are also well-behaved. Smoothed lines in Figure 6 represent running block averaging over the previous 100 MD snapshots.

Energy Decomposition. Individual energy terms which contribute to ΔG_{bind} calcd (eqs 1 and 2) were examined to determine which factors drive association and correlate best with the experimental activities and are shown in Table 2. Correlations coefficients (r^2 values) are shown for Coulombic (ΔE_{coul}), van der Waals (ΔE_{vdw}), polar ($\Delta\Delta G_{polar}$), nonpolar ($\Delta\Delta G_{nonpolar}$), total electrostatics ($\Delta G_{electro} = \Delta E_{coul} + \Delta\Delta G_{polar}$), and the total computed binding energy (ΔG_{bind} calcd $= \Delta E_{coul} + \Delta E_{vdw} + \Delta\Delta G_{polar} + \Delta\Delta G_{nonpolar}$).

As previously reported, nonbonded van der Waals interactions often correlate strongly with binding across a variety of sytems.[40,41,74–76] Representing intermolecular packing, favorable ΔE_{vdw} is a good predictor of likely intermolecular geometries. Programs such as DOCK[77] which employ scoring functions where ΔE_{vdw} terms tend to dominate have yielded good success for prediction of binding poses.[78,79] In the present study, the most potent compound S03 is computed to make the strongest ΔE_{vdw} interactions with wildtype neuraminidase compared with the other ligands ($S03_{wildtype} = -29.26$ versus ca. -21 to -24 kcal/mol, Table 2, ΔE_{vdw}). But, the trend is not maintained for the R292K mutation (Table 2, $S03_{R292K} = -22.92$ versus ca. -21 to -24 kcal/mol), and the overall correlation coefficient for

Table 2. Contributions toward Calculated Free Energies of Binding (ΔG_{bind} calcd) from MD Simulations for Sialic Acid Inhibitors (S00−S03) with Wildtype and R292K Mutant Neuraminidase Subtype N9[a]

system	ΔE_{vdw} A	ΔE_{coul} B	$\Delta\Delta G_{polar}$ C	$\Delta\Delta G_{nonpolar}$ D	$\Delta G_{electro}$ = B+C	ΔG_{bind} calcd = A+B+C+D	ΔG_{bind} expt ≈ RT ln(K_i)[b]
$S00_{wildtype}$	−23.62 &±mn; 0.09	−182.32 &±mn; 0.31	146.36 &±mn; 0.23	−4.35 &±mn; 0.002	−35.96	−64.07 &±mn; 0.13	−5.81
$S01_{wildtype}$	−21.93 &±mn; 0.09	−193.71 &±mn; 0.29	154.70 &±mn; 0.22	−4.28 &±mn; 0.002	−39.01	−65.58 &±mn; 0.11	−7.61
$S02_{wildtype}$	−22.84 &±mn; 0.11	−228.66 &±mn; 0.33	194.81 &±mn; 0.18	−4.41 &±mn; 0.002	−33.85	−61.18 &±mn; 0.14	−9.32
$S03_{wildtype}$	−29.26 &±mn; 0.10	−265.78 &±mn; 0.29	218.79 &±mn; 0.18	−4.70 &±mn; 0.001	−46.99	−81.26 &±mn; 0.15	−11.87
$S00_{R292K}$	−23.98 &±mn; 0.10	−163.63 &±mn; 0.33	145.77 &±mn; 0.27	−4.36 &±mn; 0.003	−17.86	−46.56 &±mn; 0.11	−3.74
$S01_{R292K}$	−23.31 &±mn; 0.08	−146.52 &±mn; 0.25	131.67 &±mn; 0.19	−4.37 &±mn; 0.001	−14.85	−42.85 &±mn; 0.13	−4.85
$S02_{R292K}$	−21.40 &±mn; 0.10	−185.63 &±mn; 0.29	162.95 &±mn; 0.21	−4.36 &±mn; 0.002	−22.68	−49.02 &±mn; 0.12	−6.62
$S03_{R292K}$	−22.92 &±mn; 0.10	−258.67 &±mn; 0.30	216.12 &±mn; 0.20	−4.63 &±mn; 0.001	−42.54	−70.49 &±mn; 0.13	−10.21
	$r^2 = 0.23$	$r^2 = 0.93$	$r^2 = 0.88$	$r^2 = 0.62$	$r^2 = 0.73$	$r^2 = 0.76$	

[a] All energies &±mn; standard error of the mean in kcal/mol computed from each ensemble of 2000 MD snapshots. [b] Activity values from Table 1.

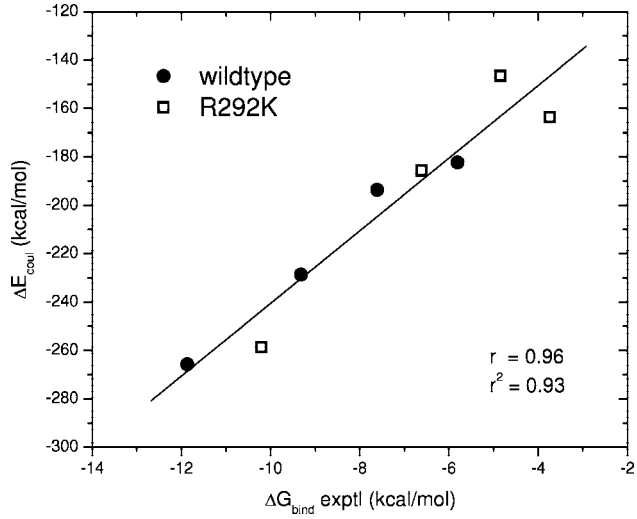

Figure 7. Correlation of nonbonded electrostatic (ΔE_{coul}) interaction energies with experimental activities (ΔG_{bind} exptl) for sialic acid inhibitors with wildtype (●) and R292K mutant (◘) neuraminidase subtype N9.

ΔE_{vdw} with experiment is low ($r^2 = 0.23$). However, the ΔE_{coul} terms are computed to be highly correlated with ΔG_{bind} exptl (Table 2) with strong overall correlation coefficients of $r = 0.96$ and $r^2 = 0.93$ (Figure 7). A least-squares fit using ΔE_{coul}, ΔE_{vdw}, $\Delta\Delta G_{polar}$, and $\Delta\Delta G_{nonpolar}$ in Table 2 as descriptors for ΔG_{bind} exptl confirms the importance of ΔE_{coul}. To obtain relative weights of the descriptors, each column of raw data in Table 2 was mean centered and scaled by the standard deviation prior to fitting. The large positive coefficient for ΔE_{coul} (1.131) vs the small coefficients obtained for other descriptors ΔE_{vdw} (0.076), $\Delta\Delta G_{polar}$ (0.094), and $\Delta\Delta G_{nonpolar}$ (−0.135) clearly indicates Coulombic energy best describes the variation. In addition, the above fit using all four terms yielded a correlation coefficient of $r^2 = 0.93$ with experiment which is the same as that obtained using only the ΔE_{coul} term alone (see Table 2).

Early studies by Taylor and von Itzstein[11] also found that electrostatic terms best described variation in activity for a series of compounds with neuraminidase of subtype N2. The Taylor study obtained $r^2 = 0.80$ using the sum of intermolecular Coulombic and reaction field free energy (computed from Poisson-Boltzmann calculations) which is comparable with the value of $r^2 = 0.73$ obtained here for the total electrostatics term ($\Delta G_{electro} = \Delta E_{coul} + \Delta\Delta G_{polar}$, Table 2). Similarly, Bonnet and Bryce[18] found that total electrostatics ($\Delta G_{electro}$) yielded the best fit with experiment ($r^2 = 0.72$, called Model 5E) for a series of 10 ligands with wildtype N9 using a MM-GBSA single-step perturbative simulation approach. As noted earlier, desolvation and Coulombic terms are highly anticorrelated (Figure 4), thus variation in $\Delta\Delta G_{polar}$ is strongly correlated with ΔG_{bind} exptl as expected ($r^2 = 0.88$). The final term, which reflects burial of surface area upon complexation for both ligand and protein ($\Delta\Delta G_{nonpolar}$), does not correlate as strongly with the activities (overall $r^2 = 0.62$, Table 2). However, $\Delta\Delta G_{nonpolar}$ is computed to be most favorable for the largest ligand S03 (−4.7 kcal/mol for WT and −4.6 kcal/mol for R292K) compared with the other ligands (ca. −4.3 to −4.4 kcal/mol) which is physically reasonable. Overall, the energetic decomposition suggests that inhibitory activity of sialic acid mimics for wildtype and the R292K mutant is primarily controlled by, and best described by, intermolecular Coulombic interactions (ΔE_{coul}). The negative sum for $\Delta G_{electro}$, which can be thought of as the intermolecular Coulombic energies mediated by the polar desolvation penalties, is generally larger in magnitude than ΔE_{vdw} (Table 2). This further suggests that electrostatics dominate association.

In contrast, Armstrong et al.[34] found that similar terms (called ΔG^{ref}_{elec} in ref 34) were positive for a series of ligands with neuraminidase and concluded that additional factors such as van der Waals, entropy, and molecular strain energies would in many cases be more significant than electrostatics. Strain effects in the NA system have been investigated previously by Masukawa et al.[16] who reported that S00 (sialic acid) could pay ca. +5 kcal/mol penalty (called $\Delta E_{internal}$ in ref 16) in going from the unbound state to the boat/twist-boat conformation observed in the bound state. Interestingly, their calculations for S01 (DANA) yielded the opposite effect with a net gain of ca. −5 kcal/mol. However, since the experimental binding difference between S00 and S01 is 1.8 kcal/mol (Table 1), which is much smaller than the ∼10 kcal/mol difference in $\Delta E_{internal}$ reported by Masukawa et al.,[16] other energy terms (i.e., ΔE_{coul}, ΔE_{vdw}, $\Delta\Delta G_{hyd}$) are clearly important. In the present study, the overall good agreement between the simulation results with experiment suggests that accounting for molecular strain is not necessary to accurately rationalize binding in this system. Differences here with

studies that suggest other terms are as or more important than ΔE_{coul} could be attributed to changes in number and type of ligands studied, the type of simulations (MD vs single-point), the type of energetic analysis (GB vs PB), or other calculation protocols. The observation that we also obtain strong correlation for $\Delta G_{electro}$ with ΔG_{bind} exptl (Table 2, $r^2 = 0.73$) reinforces the view that electrostatics both best describe variation and drive association in this system. H-bonding analysis (shown below) provides additional support. Given the highly charged nature of the NA binding site, strong agreement between ΔG_{bind} exptl and ΔE_{coul} (or with solvent mediated $\Delta G_{electro}$), as opposed to ΔE_{vdw}, is we believe physically reasonable and not unexpected.

Origins of Resistance: Binding Site Footprints. Residue-based decomposition can be used to determine hotspot regions within a binding site and reveal which specific amino acids play important roles for binding. Strockbine and Rizzo[40] recently showed the utility of using such binding site "footprints" to highlight that differential association of peptide inhibitors with HIVgp41 is driven solely by changes in ΔE_{vdw} energies occurring within a highly conserved binding pocket, supporting the hypothesis that the gp41 pocket region is an important drug target site. For the NA system, prior studies have reported a variety of residue-based methods including energy decomposition, average distances, and partial-least-squares analysis in an effort to gain insight into which inhibitor interactions are most important. [9,14,16,17,33] In the present study, Coulombic footprints were analyzed given that variation in ΔE_{coul}, as opposed to ΔE_{vdw} terms, correlates most strongly with the experimental activities ($r^2 = 0.93$, Table 2). H-bonding footprints were also computed. The primary focus here is to delineate the origins of the different fold resistance profiles for the four ligands with R292K. For the ligands with neutral functionality at position C4 (see Table 1 for numbering), Figure 8 highlights that very similar Coulombic footprints are obtained for S00 and S01, and these are both distinctly different from the corresponding footprints for ligands S02 and S03. The more rugged footprints for S00 and S01 show that many receptor residues on NA interact unfavorably (positive ΔE_{coul}) with these ligands as opposed to S02 and S03 which have much smoother ΔE_{coul} profiles and fewer per-residue energies which are unfavorable. This observation is a consequence of the fact that positively charged amine and guanidino groups on S02 and S03 lead to an overall net formal ligand charge of zero as opposed to a net negative charge for S00 and S01.

Focusing in on the key residues in the NA binding site, Figure 9 shows reduced binding footprints, defined here as the subset of residues which have a significant per-residue Coulombic energy contribution (favorable or unfavorable with $\Delta E_{coul} \geq 20$ kcal/mol). Figure 9a dramatically highlights the similar energetic profiles (ΔE_{coul}) for binding of the negatively charged S00 and S01 with wildtype NA (solid lines) versus neutral ligands S02 and S03 (dashed lines). The Figure 9a footprint quantifies the importance of the Site I central Arg (see Figure 1) at position 371 which is computed here to be the most energetically favorable interaction for each inhibitor. The relative importance of other Site I residues

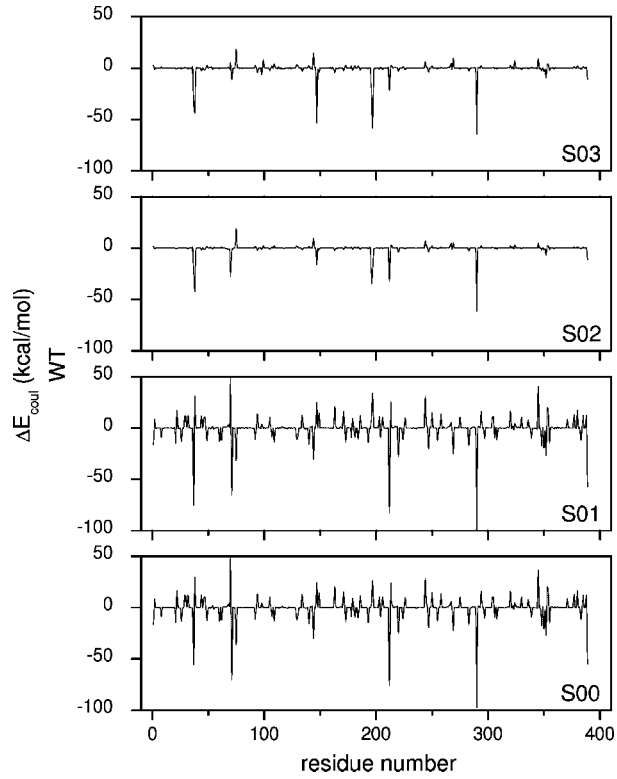

Figure 8. Intermolecular ligand−protein (per-residue) Coulombic energy footprints for wildtype N9.

R118 and R292 which flank R371 are more varied. Figure 9a also reveals that residue R292 in wildtype NA makes strong interactions with ligands S00 and S01 (ca. 80 kcal/mol), but for S02 and S03 (ca. 20−30 kcal/mol) the interaction is less significant (black arrow). Despite binding more tightly with wildtype NA (Table 1), ligands S02 and S03 do not appear to rely as strongly on electrostatic interactions with residue R292 as do S00 and S01 for their intrinsic binding affinity. Thus, the calculations suggest that any loss of interactions at position 292 would not be as detrimental for S02 and in particular S03. In general agreement with this hypothesis, experimentally, S03 loses the least amount of binding energy as a result of the R292K mutation with fold resistance $\Delta\Delta G_{R292K\text{-}WT} = 1.66$ kcal/mol compared with S02 = 2.70 kcal/mol and S01 = 2.76 kcal/mol (Table 1). Interestingly, the experimental loss in energy due to R292K for the weakest inhibitor S00 = 2.07 kcal/mol, which is less than either S01 or S02. This may be related to the suggestion that NA ligands closest in structure to the native substrate would in general be more robust to mutation.[1,80] The pyranose scaffold of S00 is saturated and most like the sialic acid moieties cleaved by NA.

Additional information about the origins of resistance becomes available when considering the differential (relative change) in Coulombic energy. Figure 9b shows the reduced per-residue Coulombic energies ($\Delta\Delta E_{coul}$) for R292K minus wildtype. Differences evident in the delta footprints reveal some enhanced interactions for S00, particularly at position D151, and R224 which probably contribute to the phenomena that the ligand is second-most robust to the mutation (Figure 9b, red solid line). The most robust inhibitor S03 shows the overall flattest profile (Figure 9b, green dashed line). Most

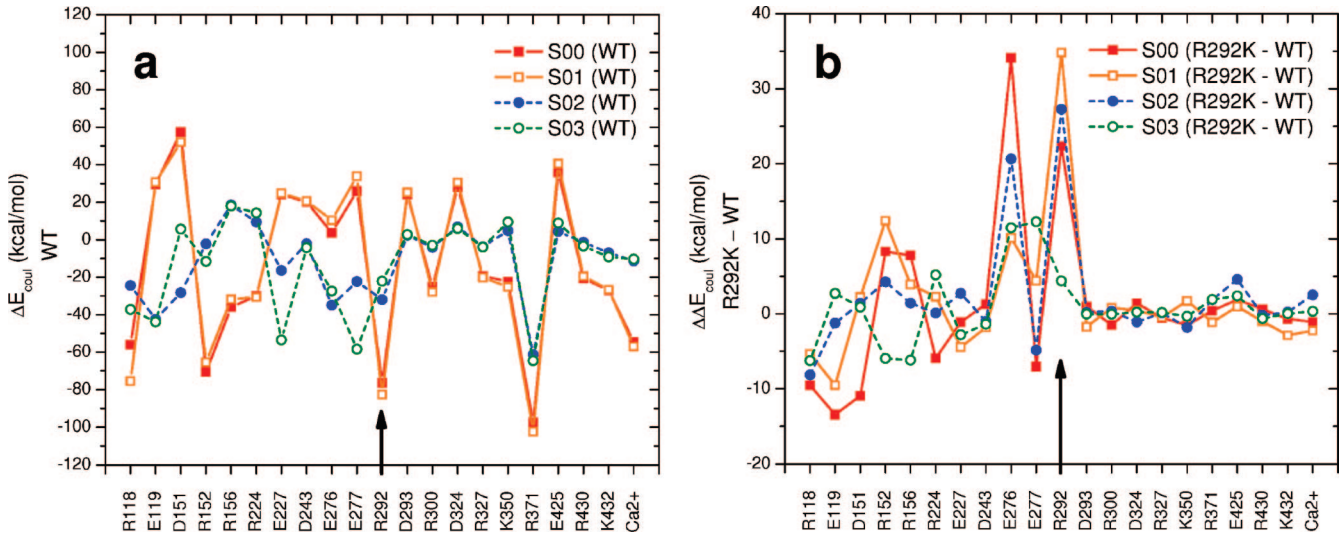

Figure 9. Intermolecular ligand-protein (per-residue) Coulombic energy footprints from a reduced set (favorable or unfavorable with $\Delta E_{coul} \geq 20$ kcal/mol). **(a)** shows the wildtype NA footprint, while **(b)** shows the difference footprint for the mutation (R292K-WT). Black arrow indicates site of the R292K mutation. Energies in kcal/mol.

significant is the fact that the change at position R292 is relatively constant for S03 compared with the other ligands (Figure 9b, black arrow). Further, the ΔE_{coul} losses here at 292 (energies in kcal/mol) for the series S03 (4.4) < S00 (22.4) < S02 (27.3) < S01 (34.8) parallel the trend for changes in experimental fold resistance (Table 1, $\Delta\Delta G_{R292K-WT}$) with S03 (1.66) < S00 (2.07) < S02 (2.70) < S01 (2.76) including the fact that S00 is second-most robust.

Compounds S02 and S03 were originally designed[1,8] using structure-based calculations (GRID program)[33] which predicted that replacement of the -OH group on S01 with positively charged functionality at position C4 on the ligand would lead to enhanced binding due to enhanced electrostatic interactions with glutamic acid at position E119 for S02 and E119 and E227 for S03. Subsequent experimental testing confirmed enhanced binding for S02 and S03 versus S01, and this is often cited as one of the premier examples of rational, computer-aided drug design. The binding footprints computed here (see Figure 9a) clearly illustrate that, as originally predicted,[8] S02 and S03 show enhanced interactions at positions E119 and that S03 makes additional favorable interactions with E227. We also note that additional favorable interactions relative to the other ligands are observed here for S03 with residue E277. As described below, the same general trends observed here for ΔE_{coul} are also seen in H-bonding footprints.

The dynamic nature of the simulations yields protein−ligand interactions with a wide-range of instantaneous per-residue energies, and such variance is expected to be biologically relevant. When viewed as histograms, the electrostatic energies shown in Figure 10 between the ligands and residue 292 only (wildtype Arg or mutant Lys) clearly show that S03 remains relatively invariant to the R292K mutation. Conversely, S00−S02 show dramatic reductions in energy and an overall shift in their respective Coulombic populations ($N = 2000$). Similarities in magnitude for energies contained in the histograms for charged (S00, S01) versus neutral (S02, S03) ligands are also noted. Overall, the ΔE_{coul} and $\Delta\Delta E_{coul}$ footprints (Figures 10–12) reveal

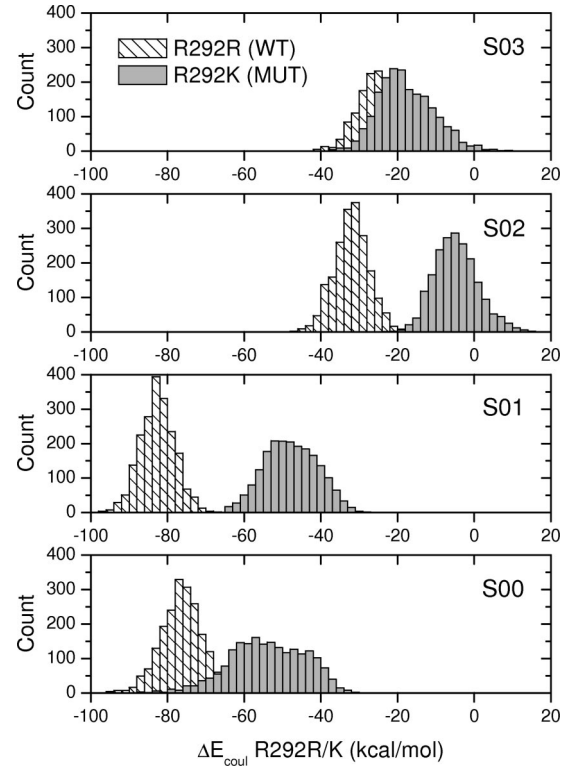

Figure 10. Populations ($N = 2000$) of per-residue Coulombic energies for ligands with residue 292 for wildtype (hashed histograms) and the R292K mutant (shaded histograms). Energies in kcal/mol.

binding differences which suggest that improved resistance is a function of less reliance on R292 for intrinsic binding affinity and enhanced binding to wildtype via specific interactions primarily at E119, E227, and E277.

Hydrogen Bonding. Given the importance that electrostatics play in this system, intermolecular hydrogen bonding was also monitored. The computed values are observed to strongly correlate with experiment. For example, average number of H-bonds from trajectories with wildtype N9 yield S00 (11.46) < S01 (12.10) < S02 (12.95) < S03 (14.23)

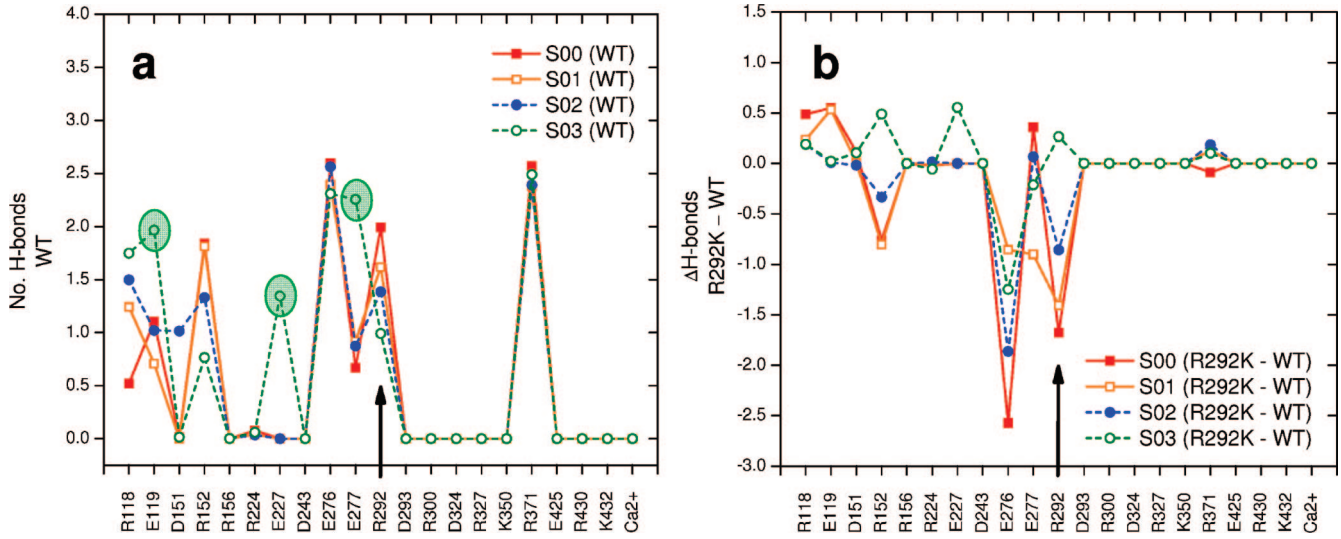

Figure 11. Hydrogen bond footprints (reduced set as in Figure 8) for ligands with NA. **(a)** shows the wildtype NA footprint, while **(b)** shows the difference footprint for the mutation (R292K - WT).

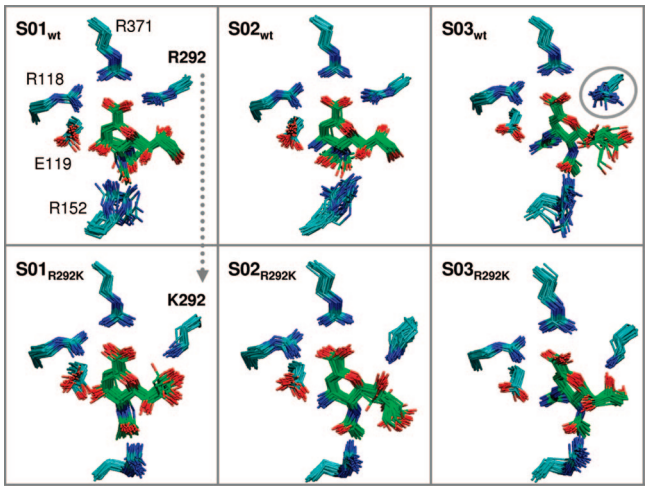

Figure 12. Comparison of snapshots from the MD trajectories of ligand S01−S03 with wildtype NA (**top**) versus the R292K mutation (**bottom**). Forty evenly spaced coordinates sets are presented with only select binding site residues shown for clarity. The arrow (left) indicates the mutation site, and the circled residue (top right panel) highlights the greater flexibility of 292 in the WT complex with S03. Ligand carbon atoms are colored green.

which parallel the binding energies order. And, H-bond values from the R292K simulations yield S00 (7.81) < S01 (8.36) < S02 (9.76) < S03 (15.13) which also follow the experimental ordering (see Table 1). The overall correlation for number of H-bonds with ΔG_{bind} exptl is $r = -0.96$, $r^2 = 0.86$. Interestingly, for R292K, a slight increase is noted for S03 compared with the dramatic losses experienced overall by the other inhibitors and is discussed further below.

Residue-based footprints were also computed to examine if changes in binding energy were structurally correlated to patterns in H-bonds. Figure 11a shows the average number of H-bonds each ligand makes with the reduced set of key pocket residues for wildtype N9. As evident in Figure 11a, all ligands are tightly coordinated to the central Site I Arg at position 371 which makes bidentate interactions with the ligand carboxylate of nearly constant 2.5 H-bonds across the series. These results are consistent with the overall architecture of the NA site (see Figure 1) and mirror the Coulombic energy trends regarding the importance of the Site I central Arg. As was similarly observed for ΔE_{coul} footprints shown in Figure 9a, H-bonding for S03 with R292 is also substantially weaker (H-bonds ca. 1.0) than for the other ligands (H-bonds >1.0) which are all more affected by the mutation. In fact, H-bonds populations at position R292 are inversely correlated to the experimental binding trends with S03 < S02 < S01 < S00 (Figure 11a, black arrow). Again, the implication is that S03 relies less on interaction with R292 for intrinsic affinity with wildtype despite the fact that the ligand is the most potent. Increased potency for S03 is a function of the dramatic increase in H-bonding with a trio of glutamic acids (E119, E227, and E277) as shown in Figure 11a (green ovals). Similar to the ΔE_{coul} profiles (Figure 9), enhanced H-bonding is a result of the much larger guanidinium group interacting with the charged glutamic acids versus smaller C4 functionality (see Table 1) for the other ligands.

Differences in per-residue hydrogen bonding (ΔH-bonds) due to R292K are shown in Figure 11b. Significant numbers of H-bonds are lost for S00−S02 and occur primarily at positions R152, E276, and R292K. At the latter position, losses of 0.9 to 1.7 interactions are observed for inhibitors S00−S02 in contrast with S03 which shows a slight gain (+0.3). The total change in intermolecular ΔH-bonds is S00 (−3.65), S01 (−3.74), S02 (−3.19), and S03 (+0.90). In general, the ΔH-bond profile in Figure 11b for inhibitor S03 is more flat compared with the other ligands as was similarly observed for the $\Delta\Delta E_{coul}$ profile shown in Figure 9.

A visual examination of MD trajectories reveals that the S03 glycerol group becomes more ordered and locked in place as a result of the mutation compared with ligands S01 and S02 which show the opposite effect (Figure 12). For S03, the R292K side chain also becomes ordered, and this probably coincides with the slight overall increase in H-bonds

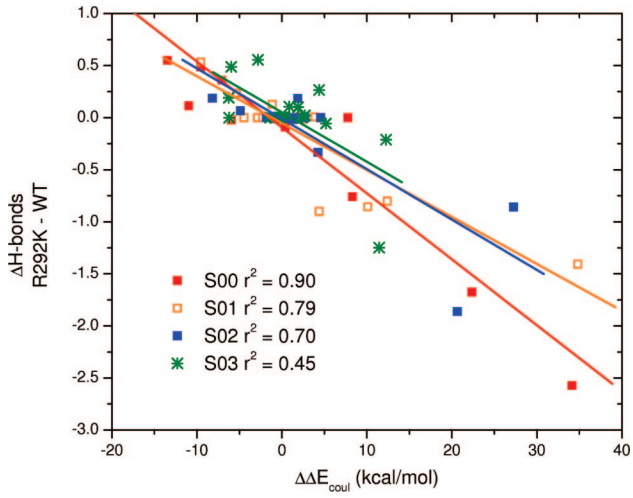

Figure 13. Correlation coefficients (r^2 values) computed between two binding site footprints, ΔH-bonds and $\Delta\Delta E_{coul}$, using the reduced set of binding site residues ($N = 21$).

for S03 as seen in Figure 11b at select positions. Interestingly, Arg 292 in wildtype simulations for S03 shows more disorder vs other ligands (Figure 12, circled residue top right panel). Greater motion here would likely lead to less H-bonds occurring with S03 at this position as is observed in Figure 11a (black arrow). And, as a consequence, S03 is expected to have less reliance on R292 for binding. Distance calculations from wildtype simulations support this hypothesis; average ligand carboxylate carbon to R292@CZ distances are larger for S03 (4.7 Å) versus S00, S01, and S02 (4.3 to 4.4 Å). At the same time, shorter distances are observed between S03 ligand scaffold atoms at position C4 (see Table 1 for numbering) and protein carboxylate atoms at position CD for residues E227 (6.0 vs 7.0 − 8.1 Å) and E277 (3.9 vs 5.4 − 5.8 Å). Here too, shortened distances are a likely consequence of stronger ΔE_{coul} (Figure 9a) and H-bonding (Figure 11a) interactions involving the S03 guanidinium group with E227 and E277.

Footprint Correlation. Finally, the similarity in some of the trends for Coulombic interaction energies and number of H-bonds suggests there may be a quantitative correlation between these descriptors. Figure 13 shows plots of ΔH-bonds vs $\Delta\Delta E_{coul}$ using the per-residue difference footprints (R292K-WT) shown in Figures 11b and 13b. Interestingly, the computed correlation coefficients (r^2 values) between these two terms inversely follow the absolute experimental binding energies with the weakest binder S00 showing the strongest correlation ($r^2 = 0.90$) followed in turn by S01 ($r^2 = 0.79$), S02 ($r^2 = 0.70$), and S03 ($r^2 = 0.45$). Inhibitors observed to lose both Coulombic energy and H-bonding at specific residues (high r^2 values) appear to rely most strongly on those residues for overall intrinsic binding versus those with flatter difference footprints (i.e., S02 and S03).

A comparison of the footprint r^2 values in Figure 13 with changes in experimental fold resistance ($\Delta\Delta G_{R292K\text{-}WT}$, Table 1) reveals a similar trend for S01 ($r^2 = 0.79$, 2.76 kcal/mol) > S02 ($r^2 = 0.70$, 2.70 kcal/mol) > S03 ($r^2 = 0.44$, 1.66 kcal/mol). However, since the weakest binder S00 actually has the second-best fold resistance value (2.07 kcal/mol), inclusion here in this pattern is not expected. Overall, the accord between r^2 values from plots of ΔH-bonds vs $\Delta\Delta E_{coul}$ with the experimental ordering (both ΔG_{bind} and $\Delta\Delta G_{bind}$) reinforces our observation that electrostatics in general is the best descriptor for understanding variation in affinity for sialic acid-based ligands with neuraminidase.

Conclusion

In this study we have employed explicit solvent all-atom MD simulations, free energy calculations, and per-residue footprint analysis to compute relative binding affinities for sialic acid-based ligands with wildtype neuraminidase subtype N9 and with a R292K mutant. The overall goal is to characterize and delineate specific origins of drug resistance. Convergence and stability of the simulations was carefully monitored through examination of instantaneous structural and energetic properties including instantaneous computed free energies of binding (Figure 6), rmsd values from starting structures, changes in desolvation energy $\Delta\Delta G_{hyd}$, and intermolecular energy components ΔE_{coul} and ΔE_{vdw} (Figure 3). Computed standard errors-of-the-mean are low (Table 2), and all measures suggest that the simulations are reasonably converged and well-behaved (Figures 3 and 6).

Notably, the MM-GBSA affinities show strong correlations with experiment (Figure 5, $r^2 = 0.76$) and in every case correctly show that loss of binding occurs as a result of the R292K mutation (Figure 6). In marked contrast to other systems,[40,41] an examination here of binding components reveal that Coulombic (ΔE_{coul}), as opposed to van der Waals (ΔE_{vdw}) energy, is the best overall descriptor for understanding variation in affinity with structure as evident by the significant correlation with experiment ($r^2 = 0.93$, Figure 7, Table 2). Conversely, ΔE_{vdw} shows little correlation ($r^2 = 0.23$). Overall, our analysis suggests that the strong correlation of ΔE_{coul} with ΔG_{bind} exptl is a consequence of the NA binding site being highly charged (Figure 1). Despite large desolvation penalties, the negative sum obtained for the $\Delta G_{electro}$ term ($\Delta E_{coul} + \Delta\Delta G_{polar}$) is in general larger in magnitude than ΔE_{vdw} (Table 2) suggesting that electrostatics is the primary driving force for association. The good correlation obtained between $\Delta G_{electro}$ and ΔG_{bind} exptl ($r^2 = 0.73$) reinforces this view.

Given the strong correlation of Coulombic energy with experiment, origins of resistance were examined through per-residue decomposition of ΔE_{coul} and H-bonding for both wildtype and difference (R292K-WT) footprints. Residue-based decomposition (Figures 11–13) reveals that the most potent ligands have (1) less reliance on R292 for intrinsic binding affinity, (2) enhanced binding via E119, E227, and E277, and (3) flatter overall ΔE_{coul} and ΔH-bond profiles. Wildtype Coulombic and H-bonding footprints confirm the importance of the Site I central Arg at position R371 for all ligands (Figures 11 and 13) and importantly reveal that S03 makes substantially weaker ΔE_{coul} (Figure 9) and H-bond (Figure 11) interactions with residue R292. Weaker interactions with R292 likely contribute to the fact that a mutation at this site is less detrimental for S03. Coulombic energy losses localized at position 292 (Figure 9b, $\Delta\Delta E_{coul}$) nicely parallel the trend for changes in experimental fold resistance energy (Table 2, $\Delta\Delta G_{R292K\text{-}WT}$) with S03 < S00 < S02 <

S01 (Table 1) including the fact S00 is second-most robust to the mutation. Conversely, more favorable interactions for S03 are observed at specific sites both in footprints for ΔE_{coul} (Figure 9a, residues E227, E277) and in footprints for numbers of H-bonds (Figure 11a, residues E119, E227, E277). Stronger per-residue interactions at these positions are a function of S03's larger guanidinium group.

Total H-bond populations for wildtype and R292K also parallel the experimental ordering ($r = -0.96$, $r^2 = 0.86$). Despite the fact S03 makes the overall largest number of H-bonds with NA, counts localized at position 292 are actually inversely correlated with experiment (Figure 11a) again suggesting S03 relies less on R292 for wildtype affinity. Upon mutation, significant numbers of total H-bonds are lost for ligands S00 (−3.26), S01 (−3.74), and S02 (−3.19), in particular at positions R152, E276, and R292K (Figure 11b). However, for S03 a slight increase in H-bonding (+0.90) is observed which can in part be traced to the fact that both residue 292 and the ligand glycerol side chain both become slightly more ordered (Figure 12). Additionally, wildtype simulations show that Arg at 292 is more disordered in simulations with S03 which helps to explain why S03 shows less H-bonding at this position (Figure 11a). Supporting this hypothesis, ligand carboxylate C1 distances with R292@CZ are longer for S03 than other inhibitors (4.7 vs 4.3 − 4.4 Å), while ligand scaffold C4 distances to E227@CD (6.0 vs 7.0 − 8.1 Å) and E277@CD (3.9 vs 5.4 − 5.8 Å) are shorter. The net result is weaker interactions for S03 with R292 and a more robust resistance profile.

The highly variable nature of the influenza virus, combined with the possibility for interspecies infection and transmission, represents a major challenge for development of both timely vaccines and development of robust antivirals active against various strains and subtypes. For this reason, studies geared toward characterization and increased understanding of how ligands bind with their antiviral targets are paramount. In this study, we have participated toward this goal by demonstrating that all-atom computer simulations with energetic and structural analysis, for a series of ligands with neuraminidase from influenza subtype N9, yield computed free energies of binding that agree well with experiment. In particular, our simulations correctly predict the effects of a known mutation at position R292K and provide clues as to origins of resistance to the mutant. Use of residue-based decomposition highlights the power of computational methods for probing specific binding interfaces and for characterization of which specific interactions govern molecular recognition. Overall, the results significantly enhance experimental observations. The likelihood of future influenza pandemics (including the possibility of highly pathogenic H5N1 strains) highlights the need for additional computational modeling studies that continue to address binding and origins of drug resistance.

Acknowledgment. Gratitude is expressed to Noel Carrascal and Rashi Goyal for computational assistance, to Janet Hearing for helpful discussions, and to the New York State Office of Science Technology and Academic Research (NYSTAR), the Office of the Vice President of Research at Stony Brook University, the Computational Science Center at Brookhaven National Laboratory, and the Stony Brook School of Medicine Targeted Research Opportunity Program for support of this research. R.C. was supported by Undergraduate Fellowships from HHMI (Award Number 52003746) and the Stony Brook URECA Program.

References

(1) von Itzstein, M. The war against influenza: discovery and development of sialidase inhibitors. *Nat. Rev. Drug Discovery* **2007**, *6*, 967–74.

(2) A revision of the system of nomenclature for influenza viruses: a WHO memorandum. *Bull. World Health Organ.* **1980**, *58*, 585–91.

(3) WHO Epidemic and Pandemic Alert and Response (EPR): Avian Influenza. http://www.who.int/csr/disease/influenza (accessed June 1, 2008).

(4) Nichol, K. L.; Treanor, J. J. Vaccines for seasonal and pandemic influenza. *J. Infect. Dis.* **2006**, *194 Suppl 2*, S111−8.

(5) Johnson, N. P.; Mueller, J. Updating the accounts: global mortality of the 1918−1920 "Spanish" influenza pandemic. *Bull. Hist. Med.* **2002**, *76*, 105–15.

(6) Rajagopal, S.; Treanor, J. Pandemic (avian) influenza. *Semin. Respir. Crit. Care Med.* **2007**, *28*, 159–70.

(7) Subbarao, K.; Klimov, A.; Katz, J.; Regnery, H.; Lim, W.; Hall, H.; Perdue, M.; Swayne, D.; Bender, C.; Huang, J.; Hemphill, M.; Rowe, T.; Shaw, M.; Xu, X.; Fukuda, K.; Cox, N. Characterization of an avian influenza A (H5N1) virus isolated from a child with a fatal respiratory illness. *Science* **1998**, *279*, 393–6.

(8) von Itzstein, M.; Wu, W. Y.; Kok, G. B.; Pegg, M. S.; Dyason, J. C.; Jin, B.; Van Phan, T.; Smythe, M. L.; White, H. F.; Oliver, S. W.; et al. Rational design of potent sialidase-based inhibitors of influenza virus replication. *Nature* **1993**, *363*, 418–23.

(9) Taylor, N. R.; von Itzstein, M. Molecular modeling studies on ligand binding to sialidase from influenza virus and the mechanism of catalysis. *J. Med. Chem.* **1994**, *37*, 616–24.

(10) Jedrzejas, M. J.; Singh, S.; Brouillette, W. J.; Air, G. M.; Luo, M. A strategy for theoretical binding constant, Ki, calculations for neuraminidase aromatic inhibitors designed on the basis of the active site structure of influenza virus neuraminidase. *Proteins: Struct., Funct., Genet.* **1995**, *23*, 264–77.

(11) Taylor, N. R.; von Itzstein, M. A structural and energetics analysis of the binding of a series of N-acetylneuraminic-acid-based inhibitors to influenza virus sialidase. *J. Comput.-Aided Mol. Des.* **1996**, *10*, 233–246.

(12) Wall, I. D.; Leach, A. R.; Salt, D. W.; Ford, M. G.; Essex, J. W. Binding constants of neuraminidase inhibitors: An investigation of the linear interaction energy method. *J. Med. Chem.* **1999**, *42*, 5142–52.

(13) Muegge, I. The effect of small changes in protein structure on predicted binding modes of known inhibitors of influenza virus neuraminidase: PMF-scoring in DOCK4. *Med. Chem. Res.* **1999**, *9*, 490–500.

(14) Wang, T.; Wade, R. C. Comparative binding energy (COMBINE) analysis of influenza neuraminidase-inhibitor complexes. *J. Med. Chem.* **2001**, *44*, 961–71.

(15) Smith, B. J.; McKimm-Breshkin, J. L.; McDonald, M.; Fernley, R. T.; Varghese, J. N.; Colman, P. M. Structural studies of the resistance of influenza virus neuramindase to inhibitors. *J. Med. Chem.* **2002**, *45*, 2207–12.

(16) Masukawa, K. M.; Kollman, P. A.; Kuntz, I. D. Investigation of Neuraminidase-Substrate Recognition Using Molecular Dynamics and Free Energy Calculations. *J. Med. Chem.* **2003**, *46*, 5628–5637.

(17) Bonnet, P.; Bryce, R. A. Molecular dynamics and free energy analysis of neuraminidase-ligand interactions. *Protein Sci.* **2004**, *13*, 946–957.

(18) Bonnet, P.; Bryce, R. A. Scoring binding affinity of multiple ligands using implicit solvent and a single molecular dynamics trajectory: Application to Influenza neuraminidase. *J. Mol. Graphics Modell.* **2005**, *24*, 147–156.

(19) Verma, R. P.; Hansch, C. A QSAR study on influenza neuraminidase inhibitors. *Bioorg. Med. Chem.* **2006**, *14*, 982–96.

(20) Amaro, R. E.; Minh, D. D.; Cheng, L. S.; Lindstrom, W. M., Jr.; Olson, A. J.; Lin, J. H.; Li, W. W.; McCammon, J. A. Remarkable loop flexibility in avian influenza N1 and its implications for antiviral drug design. *J. Am. Chem. Soc.* **2007**, *129*, 7764–5.

(21) NIH Fact Sheet. NIGMS-Supported Structure-Based Drug Design Saves Lives. http://www.nigms.nih.gov/Publications/structure_drugs.htm (accessed June 1, 2008).

(22) FDA Approved Drugs. http://www.fda.gov/cder/drug/antivirals/influenza/default.htm#drugs (accessed June 1, 2008).

(23) BioCryst Pharmaceuticals. http://www.biocryst.com/peramivir.htm (accessed June 1, 2008).

(24) Varghese, J. N.; Laver, W. G.; Colman, P. M. Structure of the influenza virus glycoprotein antigen neuraminidase at 2.9 A resolution. *Nature* **1983**, *303*, 35–40.

(25) Stoll, V.; Stewart, K. D.; Maring, C. J.; Muchmore, S.; Giranda, V.; Gu, Y. G. Y.; Wang, G.; Chen, Y. W.; Sun, M. H.; Zhao, C.; Kennedy, A. L.; Madigan, D. L.; Xu, Y. B.; Saldivar, A.; Kati, W.; Laver, G.; Sowin, T.; Sham, H. L.; Greer, J.; Kempf, D. Influenza neuraminidase inhibitors: Structure-based design of a novel inhibitor series. *Biochemistry* **2003**, *42*, 718–727.

(26) McKimm-Breschkin, J. L.; Sahasrabudhe, A.; Blick, T. J.; McDonald, M.; Colman, P. M.; Hart, G. J.; Bethell, R. C.; Varghese, J. N. Mutations in a conserved residue in the influenza virus neuraminidase active site decreases sensitivity to Neu5Ac2en- derived inhibitors. *J. Virol.* **1998**, *72*, 2456–2462.

(27) Blick, T. J.; Tiong, T.; Sahasrabudhe, A.; Varghese, J. N.; Colman, P. M.; Hart, G. J.; Bethell, R. C.; McKimm-Breschkin, J. L. Generation and characterization of an influenza virus neuraminidase variant with decreased sensitivity to the neuraminidase-specific inhibitor 4-guanidino-Neu5Ac2en. *Virology* **1995**, *214*, 475–84.

(28) Le, Q. M.; Kiso, M.; Someya, K.; Sakai, Y. T.; Nguyen, T. H.; Nguyen, K. H.; Pham, N. D.; Ngyen, H. H.; Yamada, S.; Muramoto, Y.; Horimoto, T.; Takada, A.; Goto, H.; Suzuki, T.; Suzuki, Y.; Kawaoka, Y. Avian flu: isolation of drug-resistant H5N1 virus. *Nature* **2005**, *437*, 1108.

(29) Abed, Y.; Nehme, B.; Baz, M.; Boivin, G. Activity of the neuraminidase inhibitor A-315675 against oseltamivir-resistant influenza neuraminidases of N1 and N2 subtypes. *Antiviral Res.* **2008**, *77*, 163–6.

(30) McKimm-Breschkin, J. L. Resistance of influenza viruses to neuraminidase inhibitors—a review. *Antiviral Res.* **2000**, *47*, 1–17.

(31) Zambon, M.; Hayden, F. G. Position statement: global neuraminidase inhibitor susceptibility network. *Antiviral Res.* **2001**, *49*, 147–56.

(32) Reece, P. A. Neuraminidase inhibitor resistance in influenza viruses. *J. Med. Virol.* **2007**, *79*, 1577–86.

(33) Goodford, P. J. A computational procedure for determining energetically favorable binding sites on biologically important macromolecules. *J. Med. Chem.* **1985**, *28*, 849–57.

(34) Armstrong, K. A.; Tidor, B.; Cheng, A. C. Optimal charges in lead progression: a structure-based neuraminidase case study. *J. Med. Chem.* **2006**, *49*, 2470–7.

(35) Russell, R. J.; Haire, L. F.; Stevens, D. J.; Collins, P. J.; Lin, Y. P.; Blackburn, G. M.; Hay, A. J.; Gamblin, S. J.; Skehel, J. J. The structure of H5N1 avian influenza neuraminidase suggests new opportunities for drug design. *Nature* **2006**, *443*, 45–9.

(36) De Clercq, E. Antiviral agents active against influenza A viruses. *Nat. Rev. Drug Discovery* **2006**, *5*, 1015–25.

(37) Moscona, A. Neuraminidase inhibitors for influenza. *N. Engl. J. Med.* **2005**, *353*, 1363–73.

(38) Kollman, P. A.; Massova, I.; Reyes, C.; Kuhn, B.; Huo, S.; Chong, L.; Lee, M.; Lee, T.; Duan, Y.; Wang, W.; Donini, O.; Cieplak, P.; Srinivasan, J.; Case, D. A.; Cheatham, T. E. Calculating structures and free energies of complex molecules: combining molecular mechanics and continuum models. *Acc. Chem. Res.* **2000**, *33*, 889–97.

(39) Massova, I.; Kollman, P. A. Combined molecular mechanical and continuum solvent approach (MM-PBSA/GBSA) to predict ligand binding. *Perspect. Drug Discovery Des.* **2000**, *18*, 113–135.

(40) Strockbine, B.; Rizzo, R. C. Binding of Anti-fusion Peptides with HIVgp41 from Molecular Dynamics Simulations: Quantitative Correlation with Experiment. *Proteins: Struct., Funct., Bioinf.* **2007**, *63*, 630–642.

(41) Rizzo, R. C.; Toba, S.; Kuntz, I. D. A Molecular Basis for the Selectivity of Thiadiazole Urea Inhibitors with Stromelysin-1 and Gelatinase-A from Generalized Born Molecular Dynamics Simulations. *J. Med. Chem.* **2004**, *47*, 3065–3074.

(42) Onufriev, A.; Bashford, D.; Case, D. A. Exploring protein native states and large-scale conformational changes with a modified generalized born model. *Proteins: Struct., Funct., Bioinf.* **2004**, *55*, 383–94.

(43) Feig, M.; Onufriev, A.; Lee, M. S.; Im, W.; Case, D. A.; Brooks, C. L., III. Performance comparison of generalized born and Poisson methods in the calculation of electrostatic solvation energies for protein structures. *J. Comput. Chem.* **2004**, *25*, 265–84.

(44) Rizzo, R. C.; Aynechi, T.; Case, D. A.; Kuntz, I. D. Estimation of Absolute Free Energies of Hydration Using Continuum Methods: Accuracy of Partial Charge Models and Optimization of Nonpolar Contributions. *J. Chem. Theory Comput.* **2006**, *2*, 128–139.

(45) Jorgensen, W. L. Free Energy Calculations: A Breakthrough for Modeling Organic Chemistry in Solution. *Acc. Chem. Res.* **1989**, *22*, 184–189.

(46) Kollman, P. Free Energy Calculations: Applications to Chemical and Biochemical Phenomena. *Chem. Rev.* **1993**, *93*, 2395–2417.

(47) Kormos, B. L.; Benitex, Y.; Baranger, A. M.; Beveridge, D. L. Affinity and specificity of protein U1A-RNA complex formation based on an additive component free energy model. *J. Mol. Biol.* **2007**, *371*, 1405–19.

(48) Lyne, P. D.; Lamb, M. L.; Saeh, J. C. Accurate prediction of the relative potencies of members of a series of kinase inhibitors using molecular docking and MM-GBSA scoring. *J. Med. Chem.* **2006**, *49*, 4805–8.

(49) Gohlke, H.; Case, D. A. Converging free energy estimates: MM-PB(GB)SA studies on the protein-protein complex Ras-Raf. *J. Comput. Chem.* **2004**, *25*, 238–250.

(50) Shaikh, S. A.; Ahmed, S. R.; Jayaram, B. A molecular thermodynamic view of DNA-drug interactions: a case study of 25 minor-groove binders. *Arch. Biochem. Biophys.* **2004**, *429*, 81–99.

(51) *MOE*; Chemical Computing Group: Montreal, Canada, 2007.

(52) Smith, B. J.; Colman, P. M.; Von Itzstein, M.; Danylec, B.; Varghese, J. N. Analysis of inhibitor binding in influenza virus neuraminidase. *Protein Sci.* **2001**, *10*, 689–696.

(53) *AMBER Version 8*; University of California at San Francisco: San Francisco, CA, 2004.

(54) Wang, J.; Wolf, R. M.; Caldwell, J. W.; Kollman, P. A.; Case, D. A. Development and testing of a general amber force field. *J. Comput. Chem.* **2004**, *25*, 1157–74.

(55) Hornak, V.; Abel, R.; Okur, A.; Strockbine, B.; Roitberg, A.; Simmerling, C. Comparison of multiple Amber force fields and development of improved protein backbone parameters. *Proteins: Struct., Funct., Bioinf.* **2006**, *65*, 712–25.

(56) Fornabaio, M.; Cozzini, P.; Mozzarelli, A.; Abraham, D. J.; Kellogg, G. E. Simple, intuitive calculations of free energy of binding for protein-ligand complexes. 2. Computational titration and pH effects in molecular models of neuraminidase-inhibitor complexes. *J. Med. Chem.* **2003**, *46*, 4487–500.

(57) Breneman, C. M.; Wiberg, K. B. Determining Atom-Centered Monopoles from Molecular Electrostatic Potentials - the Need for High Sampling Density in Formamide Conformational-Analysis. *J. Comput. Chem.* **1990**, *11*, 361–373.

(58) Frisch, M. J.; Trucks, G. W.; Schlegel, H. B.; Scuseria, G. E.; Robb, M. A.; Cheeseman, J. R.; Zakrzewski, V. G. ; Montgomery, J. A., Jr.; Stratmann, R. E.; Burant, J. C.; Dapprich, S.; Millam, J. M.; Daniels, A. D.; Kudin, K. N.; Strain, M. C.; Farkas, O.; Tomasi, J.; Barone, V.; Cossi, M.; Cammi, R.; Mennucci, B.; Pomelli, C.; Adamo, C.; Clifford, S.; Ochterski, J.; Petersson, G. A.; Ayala, P. Y.; Cui, Q.; Morokuma, K.; Malick, D. K.; Rabuck, A. D.; Raghavachari, K.; Foresman, J. B.; Cioslowski, J.; Ortiz, J. V.; Stefanov, B. B.; Liu, G.; Liashenko, A.; Piskorz, P.; Komaromi, I.; Gomperts, R.; Martin, R. L.; Fox, D. J.; Keith, T.; Al-Laham, M. A.; Peng, C. Y.; Nanayakkara, A.; Gonzalez, C.; Challacombe, M.; Gill, P. M. W.; Johnson, B. G.; Chen, W.; Wong, M. W.; Andres, J. L.; Head-Gordon, M.; Replogle, E. S.; Pople, J. A. *Gaussian 98, revision A.9*; Gaussian Inc.: Pittsburgh, PA, 1998.

(59) Jorgensen, W. L.; Chandrasekhar, J.; Madura, J. D.; Impey, R. W.; Klein, M. L. Comparison of Simple Potential Functions for Simulating Liquid Water. *J. Chem. Phys.* **1983**, *79*, 926–935.

(60) Berendsen, H. J. C.; Postma, J. P. M.; Vangunsteren, W. F.; Dinola, A.; Haak, J. R. Molecular-Dynamics with Coupling to an External Bath. *J. Chem. Phys.* **1984**, *81*, 3684–3690.

(61) Ryckaert, J. P.; Ciccotti, G.; Berendsen, H. J. C. Numerical-Integration of Cartesian Equations of Motion of a System with Constraints - Molecular-Dynamics of N-Alkanes. *J. Comput. Phys.* **1977**, *23*, 327–341.

(62) Darden, T.; York, D.; Pedersen, L. Particle mesh Ewald: An Nlog(N) method for Ewald sums in large systems. *J. Chem. Phys.* **1993**, *98*, 10089–10092.

(63) Tsui, V.; Case, D. A. Molecular dynamics simulations of nucleic acids with a generalized born solvation model. *J. Am. Chem. Soc.* **2000**, *122*, 2489–2498.

(64) Tsui, V.; Case, D. A. Theory and applications of the generalized Born solvation model in macromolecular simulations. *Biopolymers* **2000**, *56*, 275–91.

(65) Hawkins, G. D.; Cramer, C. J.; Truhlar, D. G. Pairwise Solute Descreening of Solute Charges from a Dielectric Medium. *Chem. Phys. Lett.* **1995**, *246*, 122–129.

(66) Hawkins, G. D.; Cramer, C. J.; Truhlar, D. G. Parametrized models of aqueous free energies of solvation based on pairwise descreening of solute atomic charges from a dielectric medium. *J. Phys. Chem.* **1996**, *100*, 19824–19839.

(67) Still, W. C.; Tempczyk, A.; Hawley, R. C.; Hendrickson, T. Semianalytical Treatment of Solvation for Molecular Mechanics and Dynamics. *J. Am. Chem. Soc.* **1990**, *112*, 6127–6129.

(68) Onufriev, A.; Bashford, D.; Case, D. A. Exploring protein native states and large-scale conformational changes with a modified generalized born model. *Proteins: Struct., Funct., Bioinf.* **2004**, *55*, 383–394.

(69) Sitkoff, D.; Sharp, K. A.; Honig, B. Accurate Calculation of Hydration Free-Energies Using Macroscopic Solvent Models. *J. Phys. Chem.* **1994**, *98*, 1978–1988.

(70) Lee, M. R.; Duan, Y.; Kollman, P. A. Use of MM-PB/SA in estimating the free energies of proteins: application to native, intermediates, and unfolded villin headpiece. *Proteins: Struct., Funct., Genet.* **2000**, *39*, 309–16.

(71) Vorobjev, Y. N.; Hermans, J. ES/IS: estimation of conformational free energy by combining dynamics simulations with explicit solvent with an implicit solvent continuum model. *Biophys. Chem.* **1999**, *78*, 195–205.

(72) Vorobjev, Y. N.; Almagro, J. C.; Hermans, J. Discrimination between native and intentionally misfolded conformations of proteins: ES/IS, a new method for calculating conformational free energy that uses both dynamics simulations with an explicit solvent and an implicit solvent continuum model. *Proteins: Struct., Funct., Genet.* **1998**, *32*, 399–413.

(73) Morozov, A. V.; Kortemme, T.; Baker, D. Evaluation of Models of Electrostatic Interactions in Proteins. *J. Phys. Chem. B* **2003**, *107*, 2075–2090.

(74) Rizzo, R. C.; Tirado-Rives, J.; Jorgensen, W. L. Estimation of binding affinities for HEPT and nevirapine analogues with HTV-1 reverse transcriptase via Monte Carlo simulations. *J. Med. Chem.* **2001**, *44*, 145–154.

(75) Rizzo, R. C.; Udier-Blagovic, M.; Wang, D. P.; Watkins, E. K.; Smith, M. B. K.; Smith, R. H.; Tirado-Rives, J.; Jorgensen, W. L. Prediction of activity for nonnucleoside inhibitors with HIV-1 reverse transcriptase based on Monte Carlo simulations. *J. Med. Chem.* **2002**, *45*, 2970–2987.

(76) Rafi, S. B.; Cui, G.; Song, K.; Cheng, X.; Tonge, P. J.; Simmerling, C. Insight through molecular mechanics Poisson-Boltzmann surface area calculations into the binding affinity of triclosan and three analogues for FabI, the E. coli enoyl reductase. *J. Med. Chem.* **2006**, *49*, 4574–80.

(77) *DOCK*; University of California at San Francisco: San Francisco, CA, 2007.

(78) Ewing, T. J.; Makino, S.; Skillman, A. G.; Kuntz, I. D. DOCK 4.0: search strategies for automated molecular docking of flexible molecule databases. *J. Comput.-Aided Mol. Des.* **2001**, *15*, 411–28.

(79) Moustakas, D. T.; Therese Lang, P. T.; Pegg, S.; Pettersen, E.; Kuntz, I. D.; Broojimans, N.; Rizzo, R. C. Development and Validation of a Modular, Extensible Docking program: DOCK 5. *J. Comput.-Aided Mol. Des.* **2006**, *20*, 601−619.

(80) Varghese, J. N.; Smith, P. W.; Sollis, S. L.; Blick, T. J.; Sahasrabudhe, A.; McKimm-Breschkin, J. L.; Colman, P. M. Drug design against a shifting target: a structural basis for resistance to inhibitors in a variant of influenza virus neuraminidase. *Struct. Fold. Des.* **1998**, *6*, 735–746.

CT800068V